Chemical Engineering Journal 526 (2025) 171196

Contents lists available at ScienceDirect

Chemical Engineering Journal

journal homepage: www.elsevier.com/locate/cej

Controlling Zn^{2+} hydration shell dynamics for long-life zinc anodes in zinc-ion energy storage

Xueqing Hu [a], Ruiqi Wu [b], Nibagani Naresh [a], Yujia Fan [a], Tianlei Wang [c], Iman Pinnock [a], Alex M. Ganose [b], Sobhit Singh [d], Ivan P. Parkin [c,*], Buddha Deka Boruah [a,*]

[a] Institute for Materials Discovery (IMD), University College London (UCL), London, WC1E 7JE, UK
[b] Department of Chemistry, Molecular Sciences Research Hub, Imperial College London, London, W12 0BZ, UK
[c] Department of Chemistry, University College London (UCL), London, WC1H 0AJ, UK
[d] Department of Mechanical Engineering, University of Rochester, New York, USA

ARTICLE INFO

Keywords:
Artificial layer
Desolvation
Zn anodes
Dendrite suppression
Zn-ion batteries and capacitors

ABSTRACT

Zinc (Zn) anodes are highly suitable candidates for aqueous rechargeable zinc-ion energy storage, offering high capacity, excellent safety, affordability, and significant potential for energy storage in mini-grid and off-grid applications. However, Zn-based anodes face challenges related to poor long-term cycling performance due to uncontrolled dendrite formation, passivation, and the hydrogen evolution reaction (HER), which occurs due to the direct interaction of water molecules with the Zn anode surface. In this study, we explore strategies for reconstructing Zn anodes by utilising 2D V_2O_5 to regulate hydrated Zn^{2+} ions and minimise the direct interaction of water molecules with Zn anodes, thereby suppressing side reactions. The V_2O_5-coated Zn (V_2O_5/Zn) anodes exhibit an extended lifespan compared to bare Zn, as well as significant dendrite-free behaviour. Theoretical simulations reveal that Zn^{2+} ion transport occurs through the interlayer spacing of V_2O_5 via the desolvation of hydrated Zn^{2+} ions. Furthermore, full-cell aqueous Zn-ion batteries (ZIBs) incorporating V_2O_5/Zn//polyaniline (PANI) configurations exhibit improved rate capability, higher capacity, and extended cycle life compared to Zn//PANI batteries. Similarly, V_2O_5/Zn anodes demonstrate enhanced long-term cycling stability and improved capacity in Zn-ion capacitors (ZICs) when paired with activated carbon cathodes, outperforming devices using pristine Zn anodes.

1. Introduction

Rechargeable lithium-ion batteries are well-established energy storage solutions due to their lightweight nature and high energy density [1,2]. However, despite their advantages, the growing demand for energy storage, particularly for large-scale applications, means that Li-ion batteries alone may not fully meet the requirements, especially when safety and cost-effectiveness are critical factors for applications such as grid-scale and mini off-grid energy storage. Aqueous zinc-ion energy storage systems offer a safer and more environmentally friendly alternative, demonstrating excellent cycling stability and lifespan [3–5]. Due to their use of aqueous electrolytes, zinc-ion energy storage systems do not require assembly in a closed environment or under inert gas conditions, and they are not highly sensitive to moisture, which significantly reduces production costs. More importantly, these systems, including batteries and capacitors, can be developed in regions where infrastructure for manufacturing air-sensitive batteries is limited, making them particularly suitable for deployment in developing countries. Moreover, zinc offers a high theoretical capacity (820 mAh g^{-1} and 5855 mAh cm^{-3}), making it promising anodes for high-performance Zn-in batteries and capacitors when paired with high-capacity cathodes [6,7]. However, despite its advantages, Zn anodes face significant challenges, including passivation, dendritic growth, corrosion, and hydrogen evolution reaction (HER), all of which impact the cycling stability of Zn-in batteries (ZIBs) and capacitors (ZICs) [8–10].

To overcome the challenges associated with Zn anodes and enhance the cycling stability of ZIBs and ZICs, various approaches have been investigated, including electrolyte engineering, the development of specialised separators [11–16], and surface modifications of the anode [3]. Among these, modifying the Zn anode surface has gained significant attention due to its relatively simple implementation and scalability in manufacturing. For example, oxide-based protective layers have been

* Corresponding authors.
E-mail addresses: i.p.parkin@ucl.ac.uk (I.P. Parkin), b.boruah@ucl.ac.uk (B.D. Boruah).

https://doi.org/10.1016/j.cej.2025.171196
Received 23 August 2025; Received in revised form 9 November 2025; Accepted 22 November 2025
Available online 23 November 2025

extensively studied as they serve as an effective shield between the Zn electrode and the electrolyte, preventing direct interaction with water molecules [3]. This protective barrier not only mitigates hydrogen evolution but also improves the Zn^{2+} deposition and dissolution process while promoting a uniform electric field. A range of oxide materials, including TiO_2 [17], ZnO [3], CeO_2 [18], $BaTiO_3$ [17], Nb_2O_5 [19], and ZrO_2 [20], have been employed as coatings on Zn anodes due to their excellent chemical and thermal stability. An artificial coating serves as a

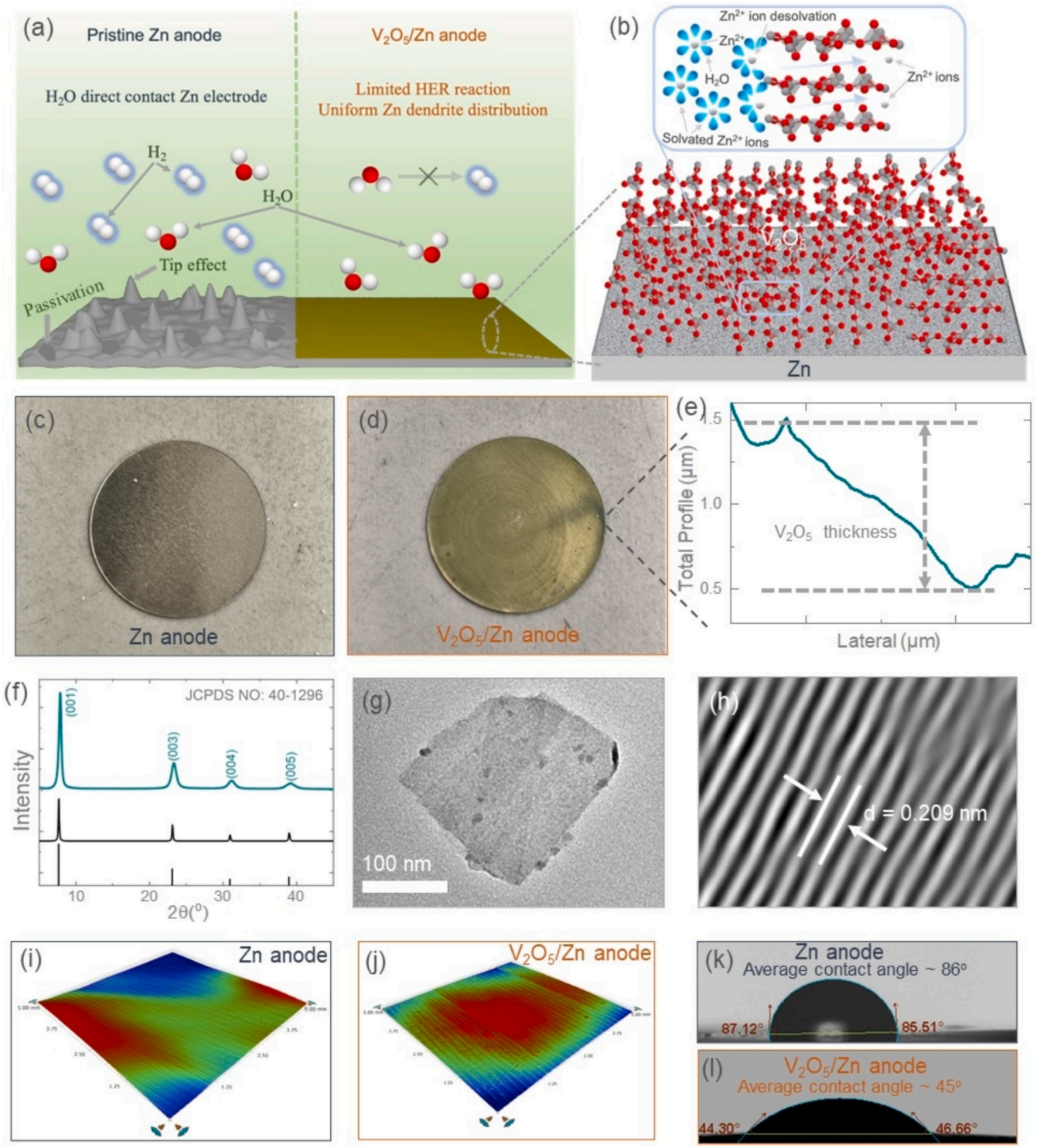

Fig. 1. (a) Schematic illustration of side reactions in a pristine Zn anode, including the tip effect, passivation, and HER, along with their suppression after surface reconstruction using Zn^{2+} compatible materials. (b) Schematic representation of Zn^{2+} ion transport through a 2D V_2O_5 coating, facilitating desolvation of hydrated Zn^{2+} ions and minimising water interaction with the anode. (c, d) Digital images of a pristine Zn anode and a V_2O_5/Zn anode. (e) Uniform 2D V_2O_5 coating on the Zn anode with an average thickness of approximately 1 μm. (f) XRD pattern of the 2D V_2O_5 nanosheet used for Zn anode coating, confirming the orthorhombic V_2O_5 a space group of Pmmn (No. 59). (g, h) TEM and HRTEM images of the 2D V_2O_5 nanosheet, with a calculated d-spacing of ~0.209 nm, corresponding to the (006) lattice plane of orthorhombic V_2O_5. (i, j) Profilometer surface morphology comparisons of pristine Zn and V_2O_5/Zn anodes. (*k*,*l*) Contact angle measurements of water droplets on pristine Zn and V_2O_5/Zn anodes, demonstrating differences in surface wettability.

shielding layer between the electrolyte and the Zn anode, reducing direct interaction and thereby decreasing the probability of HER. Furthermore, this protective layer regulates dendrite growth, ensuring a uniform formation beneath the coating while preventing dendrites from penetrating the separator, which helps mitigate the risk of short circuits. Moreover, the well-structured crystalline arrangement of the artificial layer ensures a stable and uninterrupted pathway for electron transport, enhancing the efficiency of Zn^{2+} plating and stripping.

This study introduces a unique strategy for developing dendrite-suppressing Zn anodes for high-performance ZIBs and ZICs by engineering a layered 2D V_2O_5 structure as an interfacial layer between the electrolyte and the Zn anode. The primary objective is to achieve efficiency of Zn^{2+} plating/stripping and facilitate Zn^{2+} desolvation by regulating the tunnelling of Zn^{2+} ions through the layered V_2O_5. This, in turn, minimizes water molecule interactions, thereby suppressing HER and acting as a barrier against dendrite formation. A combination of experimental investigations and theoretical calculations demonstrates that the application of a 2D V_2O_5 coating effectively inhibits dendrite growth and significantly enhances the cycling stability and capacities of Zn anodes in ZIBs and ZICs. In-situ experimental analyses further reveal that while pristine Zn anodes exhibit irregular dendrite formation, the V_2O_5-coated Zn (V_2O_5/Zn) anodes experience a notable reduction in dendrite growth, resulting in a more uniform surface even after prolonged cycling. Moreover, the fabricated full-cell ZIBs incorporating PANI cathodes not only exhibit improved cycling stability but also deliver enhanced charge storage performance when paired with V_2O_5/Zn anodes, compared to pristine Zn anodes. Similarly, ZICs using V_2O_5/Zn anodes paired with activated carbon (AC) cathodes demonstrate improved capacity and long-term cycling stability relative to those employing pristine Zn anodes with the same AC cathodes. This systematic study provides critical insights into the mechanisms governing Zn dendrite formation and underscores the potential of layered V_2O_5 structures for effective dendrite suppression, paving the way for the realization of high-performance ZIBs and ZICs.

2. Result and discussion

Fig. 1a illustrates key side reactions in ZIBs and ZICs, including the HER, the tip effect, and passivation, all of which compromise cycling stability. The tip effect results from localised electric field enhancement at sharp protrusions on the Zn anode surface, creating high-field regions that favour preferential Zn^{2+} reduction. This leads to uneven Zn deposition and dendrite formation. Passivation refers to the development of an insulating or low-conductivity layer on the Zn surface during cycling, primarily composed of zinc-based compounds. This layer hinders ion transport, charge transfer, and overall battery performance. Furthermore, water decomposition triggers HER, contributing to electrode degradation, electrolyte loss, and internal pressure build-up. As illustrated in Fig. 1b, modifying the Zn anode by coating it with artificial materials can help suppress side reactions, particularly the HER and the tip effect. However, the artificial layer must remain permeable to Zn^{2+} ions for efficient ion transport. Ideally, it should also facilitate the desolvation of hydrated Zn^{2+} ions while preventing water molecules from interacting with the Zn surface, thereby minimising unwanted side reactions. In general, solvated Zn^{2+} ions are surrounded by six water molecules, which are too large to pass through the protective artificial layer. In this study, a 2D V_2O_5 nanosheet coating is employed to effectively restrict HER by blocking water molecules from reaching the Zn electrode. Reduced HER leads to more uniform Zn deposition and mitigates the tip effect by lowering localised electric field intensity. To achieve this, we developed a simple and rapid method to directly spin-coat 2D V_2O_5 nanosheets onto zinc foil, ensuring uniform coverage of the Zn anode (Fig. S1a shows the 2D V_2O_5 ink, and Fig. S1b presents the corresponding TEM image of 2D V_2O_5; see details in the Experimental Section). Fig. 1c and d present the Zn anodes before and after spin-coating with V_2O_5, cross-sectional SEM image (Fig. S1c) and surface profile showing an average coating thickness of approximately 1 μm (Fig. 1e). The coating was set to 1 μm because thicker films developed drying-induced surface cracks, while thinner films afforded insufficient protection. Representative cracking in over-thick coatings is shown in Fig. S1d.

The X-ray diffraction (XRD) pattern of the 2D V_2O_5 nanosheets used in this study is presented in Fig. 1f. The diffraction peaks align with the standard JCPDS-40-1296 dataset, confirming the orthorhombic V_2O_5 phase with a space group of Pmmn (No. 59). The characteristic diffraction peaks observed at 7.9°, 23.3°, 31.2°, and 39.2° correspond to the (001), (003), (004), and (005) crystal planes, respectively. The transmission electron microscopy (TEM) and high-resolution TEM (HRTEM) images of the 2D V_2O_5 nanosheets are shown in Fig. 1g and h. The measured d-spacing of 0.209 nm corresponds to the (006) lattice plane of orthorhombic V_2O_5. The surface smoothness of the Zn anode plays a crucial role in the electrochemical performance of ZIBs and ZICs, as a flatter surface facilitates uniform Zn^{2+} deposition. To analyse surface changes before and after the spin-coating of 2D V_2O_5, profilometer mapping was conducted (Fig. 1i and j). The results indicate no significant variation in surface roughness after coating, apart from the 1 μm thick V_2O_5 layer, confirming a uniform coating. Moreover, the hydrophilicity of the anode surface significantly influences voltage hysteresis during Zn^{2+} deposition in aqueous electrolytes. A more hydrophilic surface reduces voltage hysteresis, lowering internal resistance. To assess this, we measured the contact angle between water and the Zn anode before and after coating with 2D V_2O_5. As shown in Fig. 1k and l, the pristine Zn anode exhibits a contact angle of approximately 86°, whereas the V_2O_5-coated Zn anode shows a reduced contact angle of ~45°. This reduction indicates enhanced surface wettability, suggesting that the V_2O_5 coating improves the Zn anode's compatibility with aqueous electrolytes, making it a more suitable choice for ZIBs.

To investigate the plating and stripping behaviour of Zn^{2+}, symmetrical coin cells were assembled using a 2 M $ZnSO_4$ electrolyte with Zn and V_2O_5/Zn anodes. Fig. 2a presents the cycling performance of Zn//Zn and V_2O_5/Zn//V_2O_5/Zn symmetrical cells at a areal current of 1 mA cm^{-2} (1 mAh cm^{-2}). The pristine Zn//Zn symmetrical cell exhibited a short circuit after just 92 h, with significant voltage fluctuations and higher internal resistance. In contrast, the V_2O_5/Zn//V_2O_5/Zn cell demonstrated a significantly longer lifespan (600 h) at the same areal current, with lower overpotential, attributed to the suppression of dendrite formation due to the V_2O_5 coating. Additionally, the V_2O_5/Zn//V_2O_5/Zn cell exhibited a lower voltage hysteresis (0.0714 V) compared to Zn//Zn (0.0805 V), which aligns with the contact angle measurements in Fig. 1k and l. Fig. 2b presents the rate performance of the symmetrical cells at various areal currents. As the areal current increased, the voltage hysteresis also increased, while reversing the areal current led to a decrease in voltage hysteresis. Across the entire current window, the Zn//Zn cell maintains a onsistently larger hysteresis than V_2O_5/Zn, reflecting higher interfacial resistance and less uniform plating/stripping on bare Zn. In contrast, the V_2O_5-coated anode exhibits lower and more stable overpotentials. Collectively, these trends demonstrate that the V_2O_5 coating delivers enhanced electrochemical stability under both low and high current rates. Besides, the voltage hysteresis for V_2O_5/Zn coin cell is significantly lower than performance observed in the current day, while results from recently reported some symmetrical cells with Zn anodes surface modification (Table S1). Although coin cells are widely used for battery testing, they may not accurately reflect the anode surface condition after cycling because the fragile glass-fiber separator can trap or tear when Zn dendrites grow into it, hindering clean separation and high-quality SEM analysis. To address this, we implemented a custom transparent cuvette clear cell configuration for symmetric Zn//Zn tests (Fig. 2c), in which both electrodes are affixed to opposite cuvette walls with a 10 mm gap and no separator, yielding a stack of electrode / large-volume electrolyte / electrode. This architecture eliminates separator interference and enables straightforward post-mortem retrieval of pristine Zn surfaces. It also differs

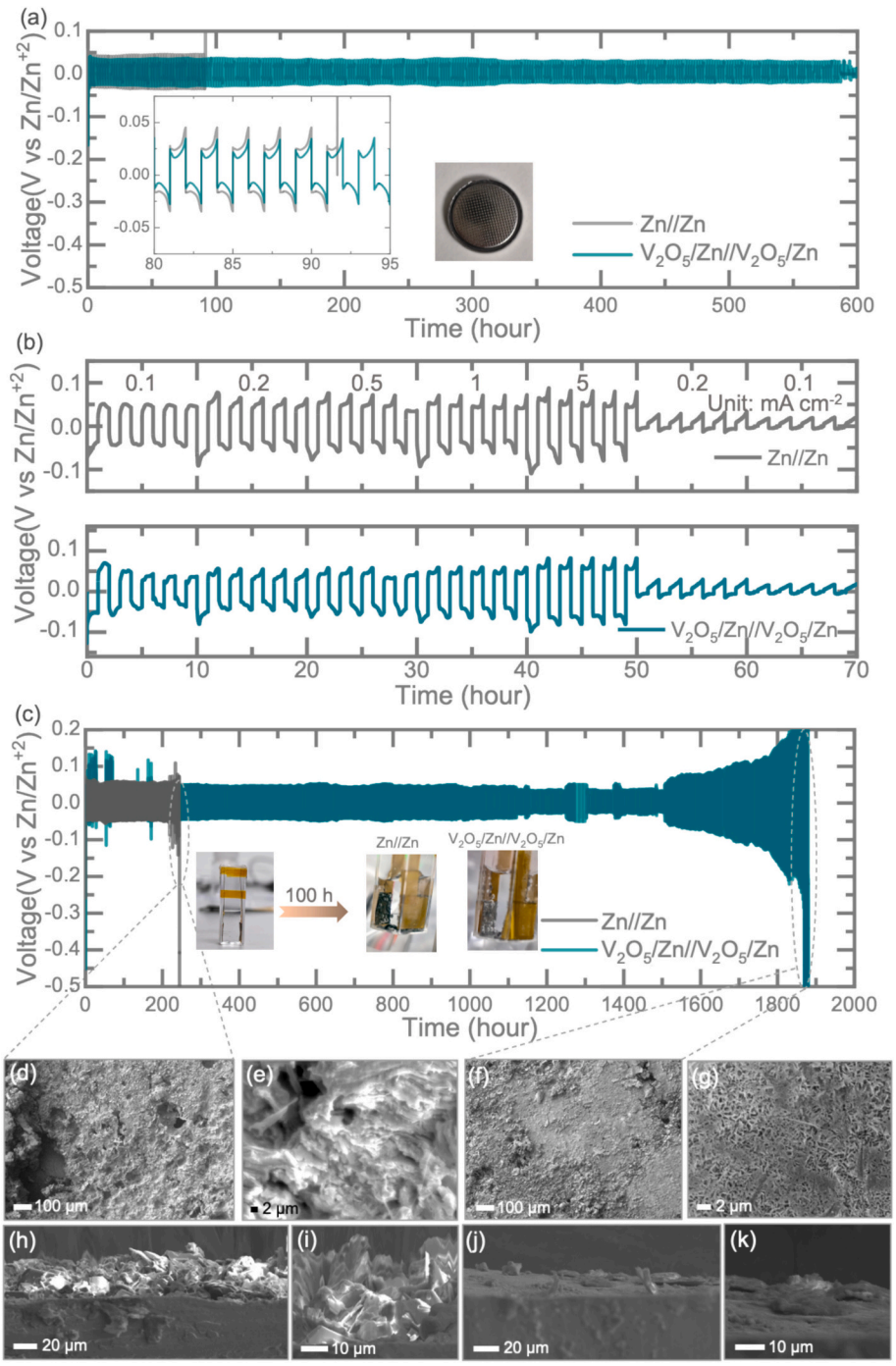

Fig. 2. (a) Comparative voltage profiles of symmetrical cells using pristine Zn and V_2O_5-coated Zn anodes, tested at an areal current of 1 mA cm^{-2} (with an areal capacity of 1 mAh cm^{-2}). (b) Rate performance evaluation of symmetrical cells under different areal currents, including 0.1 mA cm^{-2} (0.1 mAh cm^{-2}), 0.2 mA cm^{-2} (0.2 mAh cm^{-2}), 0.5 mA cm^{-2} (0.5 mAh cm^{-2}), 1 mA cm^{-2} (1 mAh cm^{-2}), and 5 mA cm^{-2} (5 mAh cm^{-2}). (c) Symmetrical cell test setup in a cuvette cell design (inset), with anodes tested at 1 mA cm^{-2}. (d, e) and (f, g) Top-view SEM images of cycled pristine Zn and V_2O_5/Zn anodes at different magnifications. The corresponding cross-sectional SEM images of pristine Zn and V_2O_5/Zn anodes are shown below (*h*–*k*).

electrochemically from traditional coin cells because there is no external stack pressure, unlike the spring-loaded contact in coin formats. Its larger electrode spacing increases solution resistance and may yield a modestly unstable initial voltage profile due to ohmic iR drop. (Fig. S2) Consequently, absolute overpotentials from the cuvette are not directly comparable to coin-cell values, while morphological trends, for example dendrite suppression, passivation, and HER signatures, remain diagnostic. To evaluate performance at high current density, we conducted symmetric-cell cycling at 5 mA cm^{-2} with an areal capacity of 5 mAh cm^{-2} (Fig. S3). Under these conditions, pristine Zn//Zn short-circuited after 40 h, whereas V_2O_5/Zn//V_2O_5/Zn sustained markedly longer stable cycling with lower hysteresis (over 280 h). To directly evaluate the reversibility of Zn deposition/stripping, we have now performed Zn//Cu and V_2O_5/Zn//Cu half-cell CE tests (Fig. S4). The V_2O_5/Zn//Cu cell sustains CE cycling for over 280 cycles, whereas the bare Zn//Cu cell fails after 199 cycles, demonstrating that the V_2O_5 coating significantly improves the reversibility and lifetime of the Zn anode. Fig. 2c displays the voltage profiles of symmetrical cells tested in cuvette cells at 1 mA

cm^{-2}. As expected, the V_2O_5/Zn cell exhibited improved stability, maintaining operation for up to 1890 h, whereas the pristine Zn cell failed after just 244 h. The corresponding SEM images of the cycled anodes, shown in Fig. 2d - g, provide further insights. Only after 244 h of cycling, the Zn anode exhibited severe surface roughness and uneven Zn deposition, indicative of uncontrolled dendrite growth and extensive side reactions (Fig. 2d and e). This ultimately led to a short circuit. Conversely, the V_2O_5/Zn anode retained a smooth and uniform surface even after 1890 h of cycling, demonstrating effective dendrite suppression. Additionally, densely packed Zn deposition was observed on the V_2O_5/Zn anode surface, suggesting enhanced Zn^{2+} ion interaction with minimal water molecule interference. Cross-sectional SEM analysis (Fig. 2h and i) further confirmed the severe dendrite growth on pristine Zn, while the V_2O_5/ Zn anode exhibited minimal surface roughness. These observations suggest that the V_2O_5 nanosheet layer effectively prevents direct water contact with the anode surface, thereby suppressing dendrite formation and improving Zn deposition uniformity.

To monitor real-time dendrite growth on Zn and V_2O_5/Zn anodes, we conducted in-situ optical monitoring in symmetrical cells, as shown in Fig. 3a. The Zn plating process was performed at a areal current of 10 mA cm^{-2} (10 mAh cm^{-2}), and cross-sectional microscope images were captured at different time intervals: 0, 15, 30, 45, and 60 min. It is

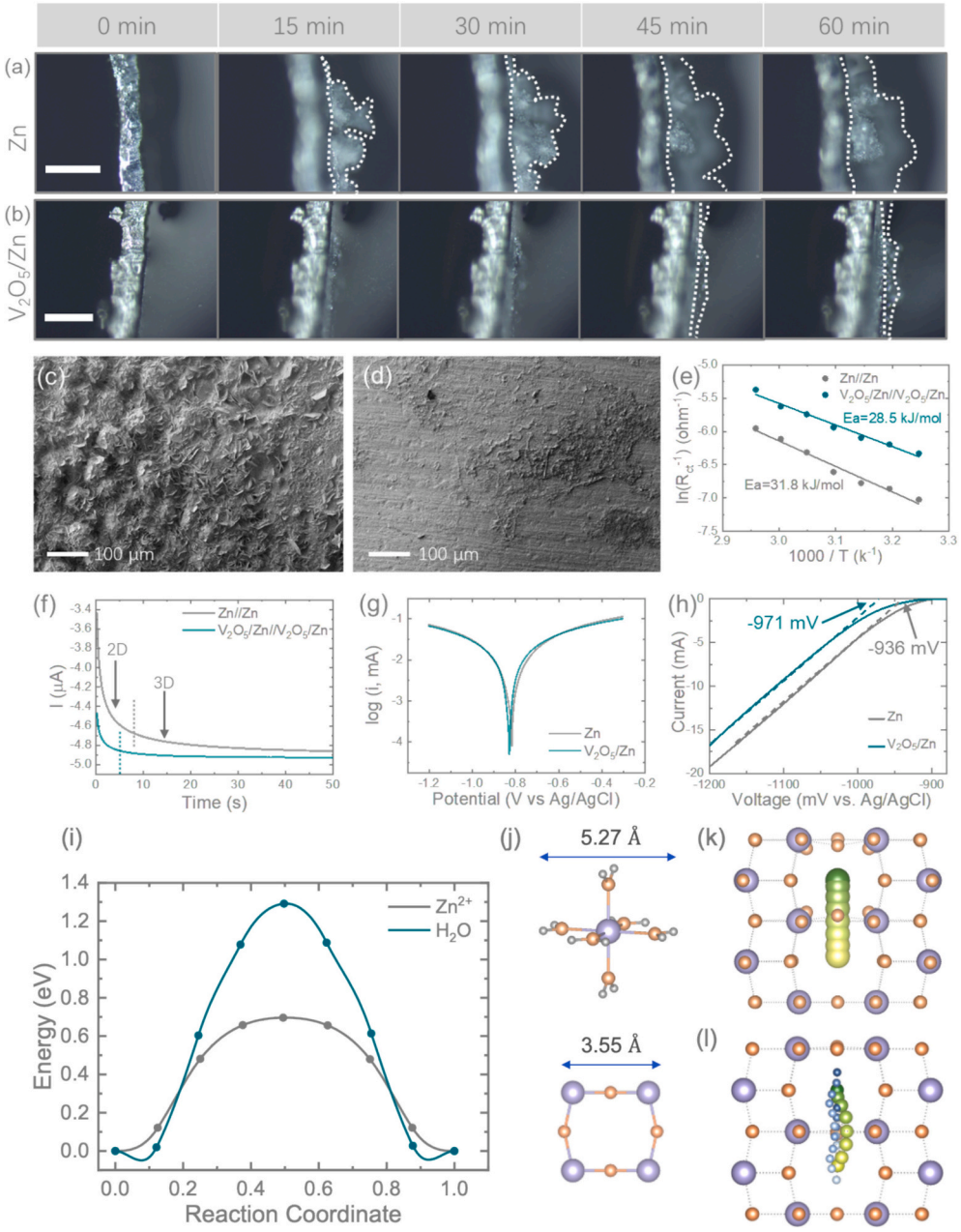

Fig. 3. (a, b) In-situ optical imaging tests of pristine Zn and V_2O_5/Zn anodes, capturing images at different Zn^{2+} deposition times (0 min, 15 min, 30 min, 45 min, and 60 min). The tests were conducted in a symmetric cell configuration at a areal current of 10 mA cm^{-2}, with a scale bar of ~200 μm. (c, d) SEM images of Zn^{2+}-plated anodes after 60 min, showing a rough surface on pristine Zn, whereas the V_2O_5/Zn anode maintains a relatively smooth morphology even after 60 min Zn^{2+} deposition. (e) Arrhenius plots comparing the activation energies of pristine Zn and V_2O_5/Zn anodes. (f) Chronoamperometry (CA) plot showing current response over time. (g) Tafel plots obtained from a three-electrode system at 0.5 mV s^{-1}, using Ag/AgCl as the reference electrode and platinum as the counter electrode. (h) Linear sweep voltammetry (LSV) curves of symmetrical cells, recorded at 0.5 mV s^{-1}, comparing the electrochemical behaviour of the anodes. The calculated transport energy barrier and trajectories for Zn ion and water diffusion in V_2O_5. (i) $Zn^{2+}$and H_2O diffusion barrier along the a lattice parameter (j) Comparision of the size of the $[Zn.6H_2O]^{2+}$ complex and V_2O_5 void (*k*,*l*) Diffusion trajectories of (k) Zn^{2+} and (l) water in V_2O_5.

evident that uncontrolled dendrite growth on the pristine Zn anode begins as early as 15 min of Zn plating, increasing significantly with plating time. The thickness of dendrites gradually expands over time (Fig. 3a). In contrast, the V_2O_5/Zn anode exhibits minimal dendrite formation (Fig. 3b), with only a few dendrites observed after 60 min of plating - significantly less than those on the pristine Zn anode. Furthermore, SEM images after 60 min of Zn plating reveal a rough and uneven surface on the pristine Zn anode (Fig. 3c), whereas the V_2O_5/Zn anode retains a smooth and uniform morphology (Fig. 3d). These results clearly demonstrate that the V_2O_5-coated Zn anode effectively suppresses dendrite formation, offering better stability compared to pristine Zn anodes. Additionally, electrochemical impedance spectroscopy (EIS) measurements were conducted at different temperatures using symmetrical cells to determine the activation energies of the anodes (Fig. S5). As shown in Fig. 3e, the activation energy values derived from Arrhenius plots are 31.8 kJ mol^{-1} for Zn//Zn and 28.5 kJ mol^{-1} for V_2O_5/Zn//V_2O_5/Zn, indicating that the V_2O_5-coated Zn anode exhibits a lower activation energy, suggesting improved charge transfer kinetics. Furthermore, the chronoamperometry (CA) plots in Fig. 3f depict the current response over time for both Zn//Zn and V_2O_5/Zn//V_2O_5/Zn cells. The pristine Zn anode exhibits a rapid two-dimensional (2D) diffusion process, with a significant current change occurring within 800 s. This behaviour suggests a rapid expansion of the specific surface area due to the uncontrolled growth of Zn^{2+} deposition. In contrast, the V_2O_5/Zn electrode effectively suppresses the 2D diffusion process, transitioning directly into a stable three-dimensional (3D) diffusion process characterised by minimal and consistent current variation. This indicates that Zn nuclei gradually evolve into a uniform Zn layer [21]. The corrosion behaviour of the anodes was further evaluated using Tafel plots from three-electrode tests (Fig. 3 g), revealing corrosion current densities of 14.8 mA cm^{-2} for pristine Zn and 13.1 mA cm^{-2} for V_2O_5/Zn. The lower corrosion current density of V_2O_5/Zn suggests enhanced corrosion resistance compared to pristine Zn. Pristine Zn and V_2O_5/Zn anode were paired with a 2 M $ZnSO_4$ electrolyte to perform linear sweep voltammetry (LSV) tests at a scan rate of 0.5 mV s^{-1}. The hydrogen evolution reaction potentials for the pristine Zn and V_2O_5/Zn anodes were determined from the tangent line of the LSV curve, measured at −936 mV and − 971 mV, respectively. These results indicate that the V_2O_5/Zn anode effectively suppresses hydrogen evolution compared to the pristine Zn anode during cycling [22]. Furthermore, we evaluated ion transport behaviour by calculating the Zn^{2+} transference number ($t_{Zn^{2+}}$) using the Bruce-Vincent method with symmetrical cells [23]. The results indicate that the transference number for the V_2O_5/Zn anode is approximately 0.79, which is significantly higher than that of the pristine Zn anode (≈0.48). This suggests a more efficient ion transfer process within the V_2O_5/Zn anode system (Fig. S6). The cyclic voltammetry (CV) curves of the V_2O_5/Zn//V_2O_5/Zn symmetrical cell exhibit a distinct redox peak of Zn^{2+}/Zn with an overpotential of approximately 56 mV. However, the overpotential of the Zn//Zn symmetrical cell is twice as high as that of the V_2O_5/Zn//V_2O_5/Zn cell (Fig. S7). This indicates that the V_2O_5/Zn electrode possesses superior electrochemical reversibility. Additionally, the increased overpotential suggests that Zn nucleation in the V_2O_5/Zn system results in finer nuclei, which can effectively suppress Zn dendrite growth [24]. To further confirm the uniform zinc deposition facilitated by the V_2O_5 coating, ex-situ XRD analysis was conducted at various charge–discharge cycles (Fig. S8). The peak intensity ratio ($I_{(002)}/I_{(101)}$) for pristine Zn increased to 0.31 and 0.37 after 5 and 20 cycles, respectively, which remained lower than those observed for V_2O_5/Zn (0.37 and 0.53). The higher peak intensity ratios in V_2O_5/Zn indicates a preferential Zn (002) orientation, suggesting more uniform zinc deposition compared to pristine Zn. Linear sweep voltammetry (LSV) was performed in a three-electrode setup using 1 M Na_2SO_4 aqueous electrolyte to eliminate interference from Zn^{2+}-related Faradaic reactions (Fig. S9). The HER onset potentials for the bare Zn and V_2O_5/Zn anodes were measured to be −1.61 V and − 1.66 V, respectively. The more negative onset potential of the V_2O_5/Zn anode indicates enhanced suppression of HER during cycling [22]. This experimental finding is strongly supported by density functional theory (DFT) calculations (see further), which reveal that V_2O_5 effectively hinders water diffusion while facilitating Zn^{2+} transport, enabling selective desolvation. The synergy between experimental data and theoretical analysis confirms that the V_2O_5 interlayer plays a critical role in mitigating HER, consistent with the observed shift in HER onset potential.

To understand the Zn ion dehydration process at the V_2O_5 coating, we conducted density functional theory simulations for Zn ion and H_2O migration (Fig. 3i). The full computational methodology is provided in the Supporting Information (Figs. S10-S12). Firstly, we note that the diameter of the $[Zn.6H_2O]^{2+}$ complex (5.27 Å) is significantly larger than the V_2O_5 void through which diffusion occurs (3.55 Å) suggesting that solvated Zn^{2+} ions will tend to desolvate before entering the V_2O_5 nanosheet (Fig. 3j). According to previous work, ion diffusion along the *a* lattice parameter (parallel to the layers) has an energy barrier nearly ten times lower than in other directions [25]. Diffusion along the *a* lattice parameter is therefore targeted in this work. We calculated Zn ion and water molecule diffusion through the V_2O_5 crystal structure via the nudged elastic band approach (Fig. 4i-l). The Zn^{2+} ion displays an energy barrier of 0.68 eV while the barrier for a single water molecule is doubled at close to 1.4 eV. Considering the exponential dependence of diffusion on the activation energy, our findings highlight that water diffusion through V_2O_5 is likely to be negligible compared to Zn ions. Accordingly, our calculations strengthen experimental insights into the role of the V_2O_5 layer in selective desolvation of hydrated Zn^{2+}. Although the V_2O_5-coated Zn shows a lower water contact angle, contact-angle measurements probe only the outermost surface and not molecular permeation through the film. Our DFT calculations indicate that intact H_2O faces a substantially higher insertion or migration barrier within the dense V—O framework than Zn^{2+}, which migrates via transient coordination with lattice oxygen. This behaviour coordinate the observations, the hydrophilic surface promotes uniform electrolyte spreading and ion flux, while the compact V_2O_5 network limits water penetration to the Zn interface, thereby suppressing H_2 evolution and dendrite formation.

Next, we evaluated the anodes by fabricating ZIB full cells with PANI cathodes, the characterisation provided in the Supporting Information (Fig. S13). Initially, we conducted cyclic voltammetry (CV) tests at varying scan rates over a voltage window of 0.5 to 1.5 V. As illustrated in Fig. S14, the CV curves of Zn//PANI and V_2O_5/Zn//PANI ZIBs both exhibit distinct pairs of redox peaks, corresponding to the interaction of Zn^{2+} ions during the charge storage process. The charge storage mechanism involves conjugated (C=N) bonds, which facilitate anion binding with oxidised PANI (C-N^+), while cations are stored at reduced PANI (C—N) sites [26,27]. Specifically, in this system, the SO_4^{2-} anion interacts with oxidised PANI during charging, whereas Zn^{2+} binds to reduced PANI during discharging. Notably, even after coating Zn with V_2O_5, the full ZIB retains similar CV curves, confirming that the charge storage mechanism remains unchanged despite the V_2O_5 modification. Additionally, Fig. S15 present the galvanostatic discharge-charge (GDC) curves recorded at different specific currents. A comparative analysis of Zn//PANI and V_2O_5/Zn//PANI ZIBs reveals that the latter demonstrates better charge storage performance. The specific capacities measured for Zn//PANI ZIBs are 74.6 mAh g^{-1} (Fig. 4a) and 66.1 mAh g^{-1} (Fig. 4b) at 1000 mAh g^{-1} and 5000 mAh g^{-1}, respectively. These values increase to 85.7mAh g^{-1} (Fig. 4a) and 72.1 mAh g^{-1} (Fig. 4b) at the same specific currents for V_2O_5/Zn//PANI ZIBs. Furthermore, the rate performance tests (Fig. 4c) of Zn//PANI and V_2O_5/Zn//PANI ZIBs confirm that the V_2O_5-coated system achieves higher specific capacities across different specific currents. The significantly enhanced specific capacity of the V_2O_5-coated anodes can be attributed to the improved uniform plating and stripping of Zn^{2+} ions as discussed earlier. Additionally, Fig. 4d illustrates the long-term cycling stability of Zn//PANI and V_2O_5/Zn//PANI ZIBs tested at 1000 mAh g^{-1}. Consistent with the GDC curves, the higher specific capacities persist over 1400 cycles, with measured values

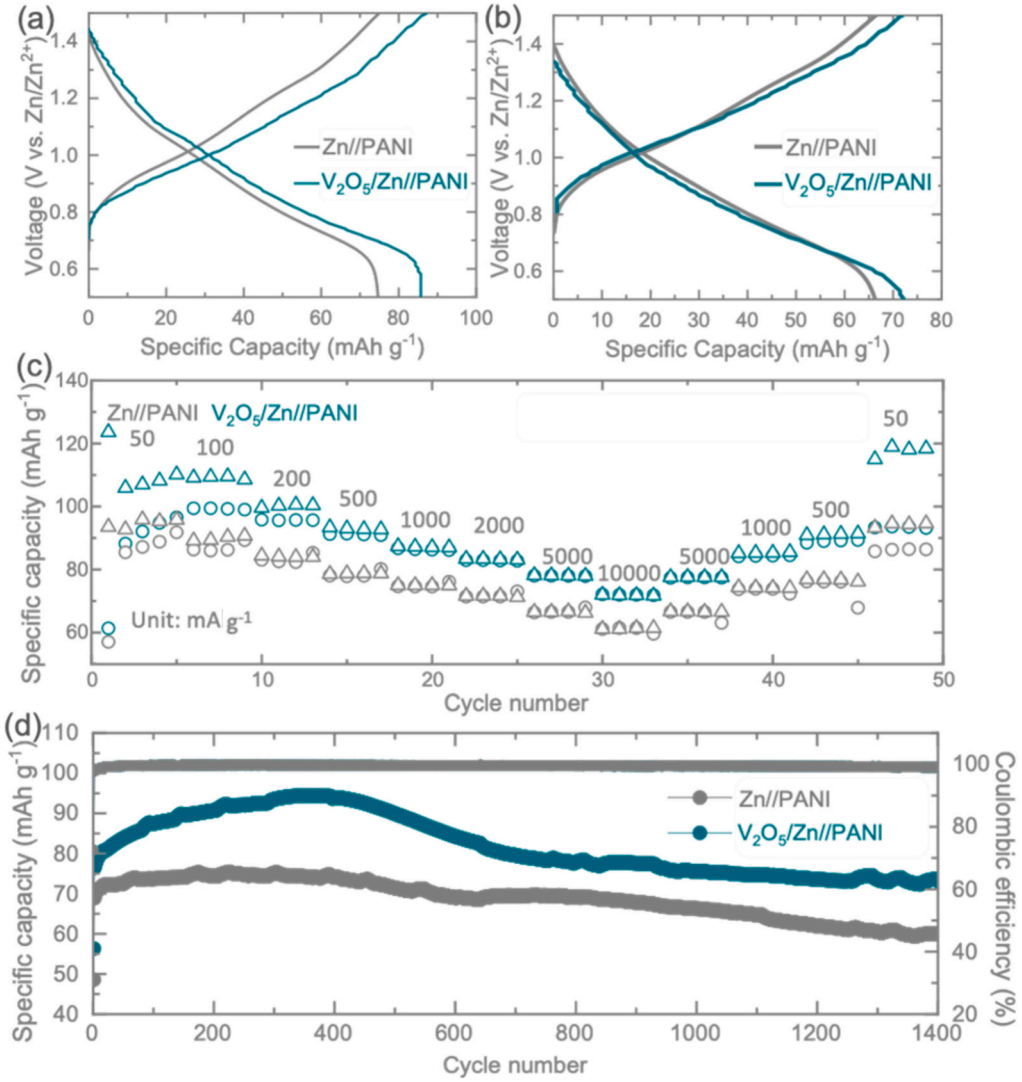

Fig. 4. (a, b) Comparative GDC profiles of Zn//PANI and V_2O_5/Zn//PANI ZIBs, tested at specific currents of 1000 mAh g^{-1} and 5000 mAh g^{-1}, respectively, within a voltage range of 0.5 to 1.5 V. (c) Rate performance evaluation of Zn//PANI and V_2O_5/Zn//PANI ZIBs at various specific currents, starting from 50 to 10,000 mA g^{-1}, followed by recovery to 50 mAh g^{-1}. (d) Long-term cycling performance of the ZIBs over 1400 cycles, showing retained specific capacities of 59.9 mAh g^{-1} and 73.3 mAh g^{-1} after cycling respectively.

of 59.9 mAh g^{-1} and 73.3 mAh g^{-1} for Zn//PANI and V_2O_5/Zn//PANI ZIBs, respectively. In addition, the V_2O_5/Zn//PANI ZIBs exhibit lower charge transfer resistance compared to the Zn//PANI ZIBs, as shown in Fig. S16. These results confirm that the V_2O_5/Zn anode not only exhibits enhanced long-term stability but also delivers improved charge-storage performance compared with the pristine Zn anode. Furthermore, as shown in Fig. S17, the V_2O_5/Zn//PANI ZIB maintained a stable voltage of approximately 1 V during self-discharge, comparable to that of typical ZIBs. This indicates that the V_2O_5 coating does not adversely affect the self-discharge behaviour, even though V_2O_5 is generally used as a cathode material in ZIBs. A thin V_2O_5 layer on the Zn anode thus has minimal impact on the self-discharge characteristics.

To further evaluate the performance of the V_2O_5/Zn anode, ZICs were assembled using pristine Zn and V_2O_5/Zn as the anode materials, paired with AC as the cathode. CV and galvanostatic charge-discharge (GCD) tests were conducted in a 1 M $ZnSO_4$ electrolyte, as shown in Fig. S18. Similar to the trends observed in ZIBs, the CV curves of ZICs revealed enhanced specific capacities with the V_2O_5/Zn anode-showing improvements of 20.3 % and 10.1 % at scan rates of 10 mV s^{-1} and 50 mV s^{-1}, respectively (Fig. 5a and b). The GCD tests confirmed this enhancement, aligning with the CV results. At specific currents of 1000 and 5000 mA g^{-1}, the Zn//AC ZICs delivered specific capacities of 36.1 and 22.2 mAh g^{-1}, respectively (Fig. 5c and d). In comparison, the V_2O_5/Zn//AC ZICs exhibited superior performance, achieving specific capacities of 50.7 and 30.7 mAh g^{-1} at the same current densities. Rate capability tests conducted from 0.05 to 10 A g^{-1} (Fig. 5e) showed that V_2O_5/Zn//AC ZICs maintained higher specific capacities - 66.3, 61.6, 56.7, 51.3, 41.1, 31.1, and 20.8 mAh g^{-1} at respective specific currents of 0.05, 0.1, 0.2, 0.5, 1, 2, 5, and 10 A g^{-1} - outperforming Zn//AC ZICs at each specific current. Moreover, cycling performance at 5 A g^{-1} (Fig. 5f) showed that after 1000 cycles, V_2O_5/Zn//AC ZICs retained a discharge capacity of 25.8 mAh g^{-1}, slightly higher than the 24.1 mAh g^{-1} of Zn//AC ZICs. Remarkably, even after 20,000 cycles, the V_2O_5/Zn//AC ZICs preserved a high specific capacity of 27 mAh g^{-1}, whereas the Zn//AC counterpart retained only 21 mAh g^{-1}. This outstanding electrochemical performance of the V_2O_5/Zn-based ZICs can be attributed to finer Zn nuclei formation, uniform Zn deposition, and suppression of dendritic growth. Moreover, Table S1 presents the galvanostatic Zn plating/stripping performance of the V_2O_5/Zn anodes developed in this work, in comparison with recently reported modified Zn anodes featuring various surface coatings. The data clearly highlight the superior stability of our V_2O_5-coated anodes relative to other coating

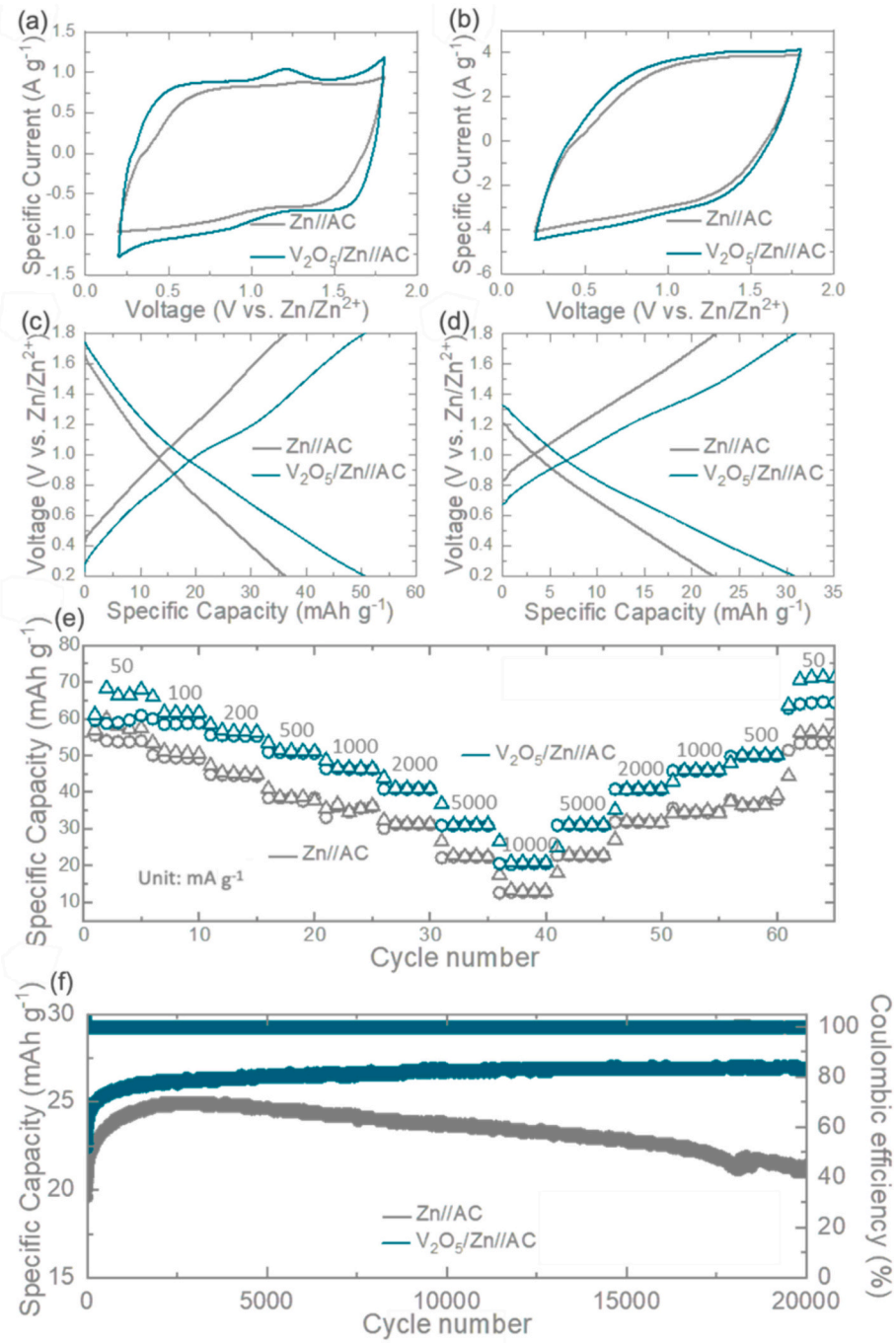

Fig. 5. Comparative CVs of the Zn//AC and V_2O_5/Zn//AC ZICs at (a) 10 mV s^{-1} and (b) 50 mV s^{-1}. Comparative GCD profiles of Zn//AC and V_2O_5/Zn//AC ZICs, tested at specific currents of (c)1000 mAh g^{-1} and (d) 5000 mAh g^{-1}, respectively, within a voltage range of 0.2 to 1.8 V. (e) Rate performance evaluation of Zn//AC and V_2O_5/Zn//AC ZICs at various specific currents, starting from 50 to 10,000 mA g^{-1}, followed by recovery to 50 mAh g^{-1}. (f) Long-term cycling performance of the Zn//AC and V_2O_5/Zn//AC ZICs tested at 5 A g^{-1}.

materials.

3. Conclusion

In conclusion, this study demonstrates a promising strategy to enhance the performance of Zn-ion-based energy storage systems - including both batteries and capacitors - by introducing a 2D V_2O_5 nanosheet artificial coating on Zn anodes. This approach effectively suppresses dendrite formation and extends cycling life. The 2D V_2O_5 layer facilitates efficient Zn^{2+} plating and stripping, reduces contact angles, and lowers activation energy, thereby improving electrochemical kinetics. Extensive experimental and theoretical analyses reveal that the artificial layer promotes Zn^{2+} desolvation and minimizes water-anode interactions, effectively suppressing the HER. As a result, V_2O_5/Zn anodes paired with PANI in ZIBs and with activated carbon in ZICs exhibit significantly enhanced charge storage performance and long-term cycling stability compared to pristine Zn anodes. Overall, our findings highlight the potential of 2D V_2O_5 nanosheets as a robust interfacial engineering solution for high-performance Zn-ion energy storage systems, offering a viable pathway toward next-generation aqueous batteries and capacitors with improved durability and capacity retention.

CRediT authorship contribution statement

Xueqing Hu: Writing – review & editing, Writing – original draft, Validation, Methodology, Investigation, Formal analysis, Data curation, Conceptualization. **Ruiqi Wu:** Writing – original draft, Validation, Investigation, Formal analysis, Data curation. **Nibagani Naresh:** Writing – original draft, Formal analysis, Data curation. **Yujia Fan:** Writing – original draft, Formal analysis, Data curation. **Tianlei Wang:** Writing – original draft, Data curation. **Iman Pinnock:** Writing – original draft, Data curation. **Alex M. Ganose:** Writing – review & editing, Writing – original draft, Supervision. **Sobhit Singh:** Writing – original draft, Validation. **Ivan P. Parkin:** Writing – review & editing, Writing – original draft, Supervision. **Buddha Deka Boruah:** Writing – review & editing, Writing – original draft, Supervision, Software, Resources, Funding acquisition.

Declaration of competing interest

The authors declare that they have no known competing financial interests or personal relationships that could have appeared to influence the work reported in this paper: Buddha Deka Boruah reports article publishing charges was provided by University College London. If there are other authors, they declare that they have no known competing financial interests or personal relationships that could have appeared to influence the work reported in this paper.

Acknowledgements

B.D.B. acknowledges support from the EPSRC research grant EP/Y008103/1.

Appendix A. Supplementary data

Supplementary data to this article can be found online at https://doi.org/10.1016/j.cej.2025.171196.

Data availability

Data will be made available on request.

References

[1] P. Albertus, V. Anandan, C. Ban, N. Balsara, I. Belharouak, J. Buettner-Garrett, Z. Chen, C. Daniel, M. Doeff, N.J. Dudney, B. Dunn, S.J. Harris, S. Herle, E. Herbert, S. Kalnaus, J.A. Libera, D. Lu, S. Martin, B.D. Mccloskey, M.T. Mcdowell, Y. S. Meng, J. Nanda, J. Sakamoto, E.C. Self, S. Tepavcevic, E. Wachsman, C. Wang, A. S. Westover, J. Xiao, T. Yersak, Challenges for and pathways toward Li-metal-based all-solid-state batteries, ACS Energy Lett. 6 (4) (2021) 1399, https://doi.org/10.1021/acsenergylett.1c00445.

[2] S. Natarajan, V. Aravindan, Burgeoning prospects of spent Lithium-ion batteries in multifarious applications, Adv. Energy Mater. 8 (33) (2018) 1802303, https://doi.org/10.1002/aenm.201802303.

[3] X.Q. Hu, J. Borowiec, Y.J. Zhu, X.P. Liu, R.Q. Wu, A.M. Ganose, I.P. Parkin, B. D. Boruah, Dendrite-free zinc anodes enabled by exploring polar-face-rich 2D ZnO interfacial layers for rechargeable Zn-ion batteries, Small 20 (18) (2023) 2306827, https://doi.org/10.1002/smll.202306827.

[4] B. Guo, J.M. Jia, Y.W. Zhao, J.L. Zhang, G.J. Li, K. Chen, A.X. Wang, C.T. Liu, Innovative zwitterionic polymers in advanced batteries, Energy Storage Mater. 78 (2025) 104253, https://doi.org/10.1016/j.ensm.2025.104253.

[5] T.T. Wang, P.J. Wang, L. Pan, Z.X. He, L. Dai, L. Wang, S.D. Liu, S.C. Jun, B.G. Lu, S.Q. Liang, J. Zhou, Stabling zinc metal anode with Polydopamine regulation through dual effects of fast Desolvation and ion confinement, Adv. Energy Mater. 13 (5) (2022) 220523, https://doi.org/10.1002/aenm.202203523.

[6] N. Zhang, X. Chen, M. Yu, Z. Niu, F. Cheng, J. Chen, Materials chemistry for rechargeable zinc-ion batteries, Chem. Soc. Rev. 49 (13) (2020) 4203–4219, https://doi.org/10.1039/C9CS00349E.

[7] Z. Yi, G. Chen, F. Hou, L. Wang, J. Liang, Strategies for the stabilization of Zn metal anodes for Zn-ion batteries, Adv. Energy Mater. 11 (1) (2021) 2003065, https://doi.org/10.1002/aenm.202003065.

[8] T. Wang, C. Li, X. Xie, B. Lu, Z. He, S. Liang, J. Zhou, Anode materials for aqueous zinc ion batteries: mechanisms, properties, and perspectives, ACS Nano 14 (12) (2020) 16321–16347, https://doi.org/10.1021/acsnano.0c07041.

[9] L. Zhang, Y. Han, Y.H. Geng, H. Zhang, H.G. Liu, Y. He, Z.C. Yan, Z.Q. Zhu, Aqueous zinc-ion batteries with boosted stability and kinetics under a wide temperature range, Angew. Chem. Int. Ed. 64 (20) (2025) 202500434, https://doi.org/10.1002/anie.202500434.

[10] J.L. Zhang, M.Y. Shi, H.W. Gao, X.X. Ren, J.C. Cao, G.J. Li, A.X. Wang, C.T. Liu, Engineering interfaces of zinc metal anode for stable batteries, Chem. Eng. J. 491 (2024) 152050, https://doi.org/10.1016/j.cej.2024.152050.

[11] Y. Zuo, K. Wang, P. Pei, M. Wei, X. Liu, Y. Xiao, P. Zhang, Zinc dendrite growth and inhibition strategies, Mater. Today Energy 20 (2021) 100692, https://doi.org/10.1016/j.mtener.2021.100692.

[12] Z. Cao, P. Zhuang, X. Zhang, M. Ye, J. Shen, P.M. Ajayan, Strategies for dendrite-free anode in aqueous rechargeable zinc ion batteries, Adv. Energy Mater. 10 (30) (2020) 2001599, https://doi.org/10.1002/aenm.202001599.

[13] L. Li, S. Jia, Z. Cheng, C. Zhang, Improved strategies for separators in zinc-ion batteries, Chem. Sus. Chem. 16 (8) (2023) 202202330, https://doi.org/10.1002/cssc.202202330.

[14] L. Wen, Z. Qiwen, H. Siru, Y. Huangming, L. Yang, C. Penghui, K. Guichao, X. Bingang, C. Yuejiao, Sustainable release of Zincophilic metal ions from separator proactively drives interfacial stabilization for durable zinc anode, Adv. Funct. Mater. 35 (32) (2025) 2425680, https://doi.org/10.1002/adfm.202425680.

[15] Y.H. Geng, W.L. Xin, L. Zhang, Y. Han, H.L. Peng, M. Yang, H. Zhang, X.L. Xiao, J. W. Li, Z.C. Yan, Z.Q. Zhu, F.Y. Cheng, Building electrode/electrolyte interphases in aqueous zinc batteries via self-polymerization of electrolyte additives, Natl. Sci. Rev. 12 (1) (2024) nwae397, https://doi.org/10.1093/nsr/nwae397.

[16] M.M. Wang, J.L. Ma, Y.H. Meng, P.Y. Tong, R.H. Luo, D.Y. Shen, X.H. Zheng, N. Chen, M.Y. Zhang, L. Song, Z.Q. Zhang, D.J. Li, C.M. Wang, H. Cheng, Y.Y. Lu, Z. Y. Li, W. Chen, In situ formation of solid electrolyte interphase facilitates anode-free aqueous zinc battery, eScience 5 (5) (2025) 100397, https://doi.org/10.1016/j.esci.2025.100397.

[17] X.Q. Hu, B. Narayan, N. Naresh, I. Pinnock, Y.J. Zhu, X.P. Liu, T.l. Wang, B. Li, I. P. Parkin, B.D. Boruah, Ferroelectric Interfaces for Dendrite Prevention in Zinc-Ion Batteries, Small 20 (49) (2024) 2403555, https://doi.org/10.1002/smll.202403555.

[18] H. Liu, J.G. Wang, W. Hua, H. Sun, Y. Huyan, S. Tian, Z. Hou, J. Yang, C. Wei, F. Kang, Building Ohmic contact interfaces toward Ultrastable Zn metal anodes, Adv. Sci. 8 (23) (2021) 2102612, https://doi.org/10.1002/advs.202102612.

[19] S. So, Y.N. Ahn, J. Ko, I.T. Kim, J. Hur, Uniform and oriented zinc deposition induced by artificial Nb_2O_5 layer for highly reversible Zn anode in aqueous zinc ion batteries, Energy Storage Mater. 52 (2022) 40–51, https://doi.org/10.1016/j.ensm.2022.07.036.

[20] Y. Liu, T. Guo, Q. Liu, F. Xiong, M. Huang, Y. An, J. Wang, Q. An, C. Liu, L. Mai, Ultrathin ZrO_2 coating layer regulates Zn deposition and raises long-life performance of aqueous Zn batteries, Mater. Today Energy 28 (2022) 101056, https://doi.org/10.1016/j.mtener.2022.101056.

[21] B.H. Liu, X. Ma, Q.H. Wang, S.L. Zhang, J. Yuwono, H.Y. Jin, J. Qiu, H.Y. Ma, C. Wang, C. Lai, Designing Copolymeric SEI layer based on click reaction toward ultralow N/P ratio and long cycle life zinc ion batteries, Adv. Energy Mater. 15 (6) (2024) 2404660, https://doi.org/10.1002/aenm.202404660.

[22] Y.F. Huang, Z.W. Chang, W.B. Liu, W.T. Huang, L.B. Dong, F.Y. Kang, C.J. Xu, Layer-by-layer zinc metal anodes to achieve long-life zinc-ion batteries, Chem. Eng. J. 431 (2022) 133902, https://doi.org/10.1016/j.cej.2021.133902.

[23] L. Yang, Y.J. Zhu, H.P. Yu, Z.Y. Wang, L. Cheng, D.D. Li, J.C. Tao, G. He, H. Li, A five Micron thick aramid nanofiber separator enables highly reversible Zn anode for energy-dense aqueous zinc-ion batteries, Adv. Energy Mater. 14 (39) (2024) 2401858, https://doi.org/10.1002/aenm.202401858.

[24] S. Bhoyate, S. Mhin, J. Jeon, K.R. Park, J.Y. Kim, W.B. Choi, Stable and high-energy-density Zn-ion rechargeable batteries based on a MoS_2-coated Zn anode, ACS Appl. Mater. Interfaces 12 (24) (2020) 27249–27257, https://doi.org/10.1021/acsami.0c06009.

[25] Y. Lu, H. Andersen, R. Wu, A.M. Ganose, B. Wen, A. Pujari, T. Wang, J. Borowiec, I. P. Parkin, M.D. Volder, B.D. Boruah, Hydrogenated V_2O_5 with improved optical and electrochemical activities for photo-accelerated Lithium-ion batteries, Small 20 (14) (2024) 2308869, https://doi.org/10.1002/smll.202308869.

[26] F. Wan, L.L. Zhang, X.Y. Wang, S.S. Bi, Z.Q. Niu, J. Chen, An aqueous rechargeable zinc-organic battery with hybrid mechanism, Adv. Funct. Mater. 28 (45) (2018) 1804975, https://doi.org/10.1002/adfm.201804975.

[27] P. Jiménez, E. Levillain, O. Alévêque, D. Guyomard, B. Lestriez, J. Gaubicher, Lithium n-doped polyaniline as a high-performance electroactive material for rechargeable batteries, Angew. Chem. Int. Ed. 56 (6) (2017) 1553–1556, https://doi.org/10.1002/anie.201607820.